Electrodeposition of Textured Ceramic Superlattices in the Pb−Tl−O System

Richard J. Phillips, Teresa D. Golden, Mark G. Shumsky, Eric W. Bohannan, and Jay A. Switzer*

University of Missouri−Rolla, Department of Chemistry, and Graduate Center for Materials Research, Rolla, Missouri 65409-1170

Received February 5, 1997. Revised Manuscript Received May 5, 1997[⊗]

Superlattices in the Pb−Tl−O system were electrodeposited at room temperature from aqueous solution. The deposition solution was 0.005 M Tl(I) and 0.100 M Pb(II) in 5 M NaOH. The superlattices grew epitaxially on oriented prelayers with either a [100] or [210] texture. The out-of-plane texture of the prelayer was maintained throughout the growth of the superlattice. X-ray diffraction (XRD) showed the films to be superlattices by the presence of satellites around the main Bragg reflections. There was good agreement between XRD and scanning tunneling microscopy for the measurement of modulation wavelengths from 3 to 150 nm. Partial relaxation of coherency was observed for modulation wavelengths exceeding about 20 nm.

Introduction

Superlattices are an example of a nonequilibrium structure that can be assembled electrochemically. The low processing temperature of electrodeposition should allow the growth of nanoscale architectures with minimal interdiffusion across interfaces. Electrodeposition also provides feedback during the deposition process, since the current during a potentiostatically controlled deposition provides a measure of the deposition rate. We have previously analyzed the current−time transients during the deposition of a superlattice to estimate the composition profile in the nanometer-scale layers.[1]

Most research on the electrodeposition of superlattices has been on metallic systems.[2] The emphasis has been on growing nanoscale structures with enhanced elastic and plastic properties,[3,4] improved wear resistance,[5] and magnetic anisotropy.[6] Schwarzacher has grown modulated nanoscale wires for giant magnetoresistance applications.[7,8]

Our interest lies in the deposition of nanometer-scale metal oxides with optical or electrical properties which are a function of the dimension of the material. We have shown that it is possible to electrodeposit Cu_2O,[9] Cu_2O/Cu nanocomposites,[10] AgO,[11] nanophase CeO_2,[12] and ZrO_2,[13] epitaxial $Ag(Ag_3O_4)_2NO_3$,[14] compositional superlattices of Pb−Tl−O,[15,16] and defect-chemistry superlattices based on Tl_2O_3.[17] In this paper we provide details on the electrodeposition and characterization of superlattices in the Pb−Tl−O system with a strong out-of-plane preferred orientation.

Experimental Section

Electrochemical experiments were performed using an EG&G Princeton Applied Research (PAR) model 273A potentiostat/galvanostat. A constant temperature was maintained at 25 °C by a Fisher Scientific Model 9100 circulator, and the solutions were stirred. The current response during superlattice deposition was recorded with a Nicolet Model 310 digital oscilloscope. The cell configuration consisted of the platinum counter electrode placed horizontally approximately 1 cm below a horizontal stainless steel working electrode. A standard calomel reference electrode within a bridge tube solution of 5 M $NaNO_3$ was placed approximately 1 cm from the working electrode. A polyethylene frit was used at the end of the bridge tube. The working electrode was a 430 stainless steel disk (electrode area = 1.96 or 3.88 cm^2) supplied by Metal Samples, Inc. A platinum rotating disk electrode (area = 0.138 cm^2) was used as the working electrode for the linear sweep experiments. Contact was made to the electrode by attaching a copper wire to the back face of the electrode using silver epoxy available from Epoxy Technology, Inc. (415G). The electrode resistance was 0.5 Ω or less between the exposed face of the electrode and the copper wire. Once the silver epoxy was cured for 24 h, the electrode was mounted in Buehler epoxide resin (20-8130-128) and epoxide hardener (20-8132-032) in a 5:1 resin to hardener ratio, followed by a 24 h cure. The electrode was then polished by wet grinding through Buehler Carbimet 600 grit SiC paper. Final polishing was performed on Buehler Microcloth (40-7218) through 0.05

* To whom correspondence should be addressed.

[⊗] Abstract published in *Advance ACS Abstracts,* June 15, 1997.

(1) Switzer, J. A.; Phillips, R. J.; Golden T. D. *Appl. Phys. Lett.* **1995**, *66*, 819.
(2) Moffat, T. P. *J. Electrochem. Soc.* **1995**, *142*, 3767.
(3) Tench, D. M.; White, J. T. *J. Electrochem. Soc.* **1990**, *137*, 3061.
(4) Lashmore, D. S.; Thomson, R. *J. Mater. Res.* **1992**, *7*, 2379.
(5) Ruff, A. W.; Lashmore, D. S. *Wear* **1991**, *151*, 245.
(6) McMichael, R. D.; Atzmony, U.; Beauchamp, C.; Bennett, L. H.; Swartzendruber, L. J.; Lashmore, D. S.; Romankiw, L. T. *J. Magn. Magn. Mater.* **1992**, *113*, 149.
(7) Schwarzacher, W.; Lashmore, D. S. *IEEE Trans. Magn.* **1996**, *32*, 3133.
(8) Attenborough, K.; Hart, R.; Schwarzacher, W.; Ansermet, J.-P. *Mater. Res. Soc. Symp. Proc.* **1995**, *384*, 3.
(9) Golden, T. D.; Shumsky, M. G.; Zhou, Y.; VanderWerf, R. A.; Van Leeuwen, R. A.; Switzer, J. A. *Chem. Mater.* **1996**, *8*, 2499.
(10) Switzer, J. A.; Hung, C.-J.; Bohannan, E. W.; Shumsky, M. G.; Golden, T. D.; VanAken, D. C. *Adv. Mater.* **1997**, 9, 334.
(11) Breyfogle, B. E.; Hung, C.-J.; Shumsky, M. G. Switzer, J. A. *J. Electrochem. Soc.* **1996**, *143*, 2741.
(12) Zhou, Y.; Phillips, R. J.; Switzer, J. A. *J. Am. Ceram. Soc.* **1995**, *78*, 981.
(13) Switzer, J. A.; Phillips, R. J. *Mater. Res. Soc. Symp. Proc.* **1988**, *121*, 111.
(14) Breyfogle, B. E.; Phillips, R. J.; Switzer, J. A. *Chem. Mater.* **1992**, *4*, 1356.
(15) Switzer, J. A.; Shane, M. J.; Phillips, R. P. *Science* **1990**, *247*, 444.
(16) Switzer, J. A.; Raffaelle, R. P.; Phillips, R. J.; Hung, C.-J.; Golden, T. D. *Science* **1992**, *258*, 1918.
(17) Switzer, J. A.; Hung, C.-J.; Breyfogle, B. E.; Shumsky, M. G.; Van Leeuwen, R.; Golden, T. D. *Science* **1994**, *264*, 1505.

S0897-4756(97)00074-4 CCC: $14.00

μm alumina. The electrode was rinsed with distilled water and ultrasonicated between each grinding/polishing stage. This epoxy mounting procedure produced a stainless steel disk flush with the surface of the epoxy, allowing more uniform mass transport control across the surface of the working electrode in a stirred solution.

The Pb−Tl−O prelayers and superlattices were deposited from 0.005 M $TlNO_3$ and 0.1 M $Pb(NO_3)_2$ in 5 M NaOH (**caution**: thallium and lead compounds are extremely toxic). Tl_2O_3 prelayers were deposited from 0.1 M $TlNO_3$ in 5 M NaOH. The 5 M NaOH was prepared in deionized water. With this solution still warm, the nitrate salts were added, and the solution was allowed to cool and age for 24 h before deposition. The aging (while stirring) of the solution was needed to completely dissolve the salts in solution. The prelayers were grown to 20 and 5 μm for the Pb−Tl−O and Tl_2O_3, respectively. Subsequent superlattice growth on these prelayers did not result in a change of the texture throughout the thickness of the superlattice. The mixed oxide prelayers were deposited from a fresh stirred solution each time to minimize the effects of thallium ion depletion from the solution. All solutions were made from reagent grade chemicals dissolved in doubly distilled deionized water with a resistivity of at least 18 MΩ cm.

Compositions of Pb−Tl−O films were analyzed with a JEOL JSM-T330A scanning electron microscope using energy-dispersive X-ray spectroscopy. The accelerating voltage was 20 keV with a 90° beam incident angle, 29.9° X-ray emergence angle, 0.5° X-ray window incidence angle, a channel to channel separation of 20 eV, and a data acquisition time of 100 s. The L-lines were used from the energy spectrum for analysis.

X-ray diffraction patterns were run on a Scintag 2000 diffractometer using Cu Kα radiation ($\lambda_{K\alpha 1} = 0.154\ 059\ 8$ nm). The tube source was operated at 45 kV and 40 mA. Two types of diffraction experiments were performed. The first was a symmetric scan used to evaluate the film texture and modulation wavelength perpendicular to the substrate. The second type of scan was used to determine the texture parallel to the substrate. Symmetric scans which were used to determine the overall texture utilized a step of 0.02° in 2 θ, with a 1 s dwell time per step. To obtain improved statistics around the satellite positions for the superlattice films, a step of 0.02° in 2 θ with a 10 s dwell time was used. The source slit widths were 1.0 mm and 2.0 mm. The detector was a Si−Li solid-state detector maintained at 77 K, with two receiving slits of 0.5 and 0.3 mm widths. Scans to evaluate the texture parallel to the substrate were run at a step of 0.1° and a 1 s dwell time per step.

Scanning tunneling microscopy experiments were performed directly in air on cleaved cross sections of the Pb−Tl−O superlattice with a Digital Instruments Nanoscope II. Mechanically formed Pt/Ir tips were used as probes. All measurements were obtained with a bias voltage of 200 mV (sample positive), tunneling current of 0.5 nA, and scan rate of 4.34 Hz.

Results and Discussion

Linear Sweep Voltammetry. The composition of an individual layer can be controlled during electrodeposition by having the solution concentration of the species which is oxidized at the lowest potential kept low and a separation between the standard reduction potentials of the individual components. For deposition of mixed metal Pb−Tl−O films, the [Tl(I)] is kept low in solution (5 mM), while [Pb(II)] is much higher (100 mM). The solution for mixed oxide deposition is compared to the individual solutions of 5 mM $TlNO_3$ in 5 M NaOH and 0.1 M $Pb(NO_3)_2$ in 5 M NaOH using linear sweep voltammetry as shown in Figure 1. This shows that the open-circuit potentials (potential at zero current) of the individual solutions of Pb(II) and Tl(I) are separated by over 200 mV. Also, for a 5 mM Tl(I) concentration, a mass-transport-limited current density of 2.3 mA/cm^2 was measured. The linear sweep voltammetry indicates that for the range of potentials used to deposit the superlattices, the Tl(I) deposition is mass-transport-limited. Since a mass transport limited current is not observed for Pb(II), this component is deposited under activation or kinetic control.

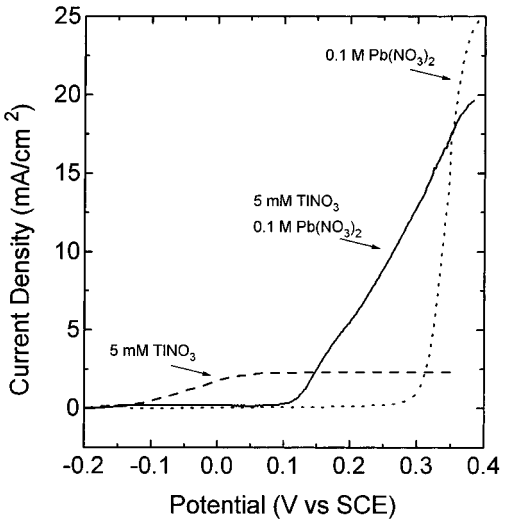

Figure 1. Linear sweep voltammetry for individual and multiple component solutions. The supporting electrolyte was 5 M NaOH in a stirred solution. The scan rate was 10 mV/s.

For the linear sweep curves in Figure 1, the sum of the currents from the individual solutions do not add up to the measured current for the mixed solution. The current from the mixed solution increases above the mass transport limited current for Tl(I) approximately 150 mV before the oxidation of Pb(II) was observed in the 0.1 M $Pb(NO_3)_2$ solution. Also, the current in the mixed solution appears to be suppressed, and the Tl(I) mass-transport-limited current obtained in the 5 mM $TlNO_3$, 5 M NaOH solution is not observed in the mixed solution before 150 mV vs SCE. A possible explanation for the voltammetry results of the mixed Pb−Tl solution could be the result of adsorbed Pb(II) species. Fleischmann et al.[18] proposed a mechanism for the deposition of PbO_2, where adsorbed $Pb(OH)^{+}_{2,ads}$ or $Pb(OH)^{2+}_{2,ads}$ were involved in the rate-determining steps in the deposition. The adsorbed species may be responsible for the decreased current of the mixed solution before 150 mV vs SCE. A similar shifting of the deposition potentials for the mixed oxide was also observed by cyclic voltammetry.[19]

To examine the effect of Pb(II) on the deposition of Tl(I), we added varying amounts of $Pb(NO_3)_2$ to a 5 mM $TlNO_3$, 5 M NaOH solution. Figure 2 shows the linear sweep voltammetry results for stirred solutions of 5 mM $TlNO_3$ in 5 M NaOH with varying amounts of Pb(II) added to the Tl(I) solution. Curve A shows the linear sweep with no Pb(II) in solution. As the concentration of Pb(II) is increased, the current tends to rise more rapidly for a given applied potential (i.e., solutions B and C). A further increase in the Pb(II) concentration to 5 mM (i.e., solution D) results in a current rise similar to a solution without Pb(II) (i.e., solution A). An increase in the limiting current from 2.3 mA/cm^2 for 0 mM Pb(II) to 4.7 mA/cm^2 for 5 mM Pb(II) is observed. As the concentration of Pb(II) is increased to 75 mM (solution E) and 100 mM (solution F), a definitive Tl(I) limiting current is not observed, and the voltammogram

(18) Fleischmann, M.; Thirsk, H. R. *Electrochim. Acta* **1960**, *2*, 22.
(19) Voos, B.; Pleth, W.; Borner, R. H. K.; Schollhorn, R. *Electrochim. Acta* **1993**, *38*, 2551.

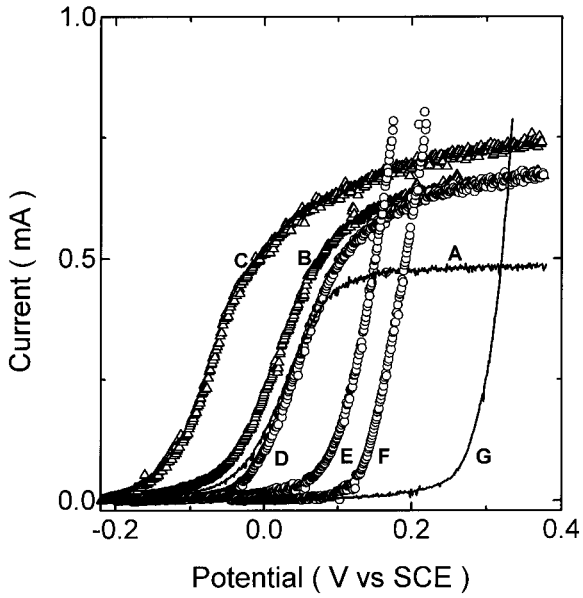

Figure 2. Linear sweep voltammetry for a 5 mM $TlNO_3$, 5 M NaOH stirred solution with (A) 0 mM, (B) 0.01 mM, (C) 1.0 mM, (D) 5.0 mM, (E) 75 mM, and (F) 100 mM $Pb(NO_3)_2$. Solution (G) is 100 mM $Pb(NO_3)_2$ in 5 M NaOH. The scan rate was 10 mV/s and the electrode area 0.138 cm^2.

Table 1. Summary of Open-Circuit Potentials for 1 μm Thick Tl_2O_3, $Pb_xTl_yO_z$, and PbO_2 Films in a Solution of 5 MM $TlNO_3$, 100 MM $Pb(NO_3)_2$, and 5 M NaOH

applied potential (mV vs SCE)	open-circuit potential (mV vs SCE)	atomic percent[d]	
		Tl	Pb
80[a]	−15	100	0
70[b]	−5	55	45
120[b]	15	42	58
150[b]	22	36	64
230[b]	51	24	76
260[b]	56	18	82
295[c]	60	0	100

[a] Deposited from 100 mM $TlNO_3$, 5 M NaOH, stirred. [b] Deposited from 5 mM $TlNO_3$, 100 mM $Pb(NO_3)_2$, 5 M NaOH, stirred. [c] Deposited from 100 mM $Pb(NO_3)_2$, 5 M NaOH, stirred. [d] Determined on a metals-only basis.

shifts toward a solution containing only 100 mM Pb(II) (solution G).

The open-circuit potentials were measured in a mixed solution of 5 mM $TlNO_3$, 100 mM $Pb(NO_3)_2$, and 5 M NaOH for 1 μm thick Tl_2O_3, $Pb_xTl_yO_z$, and PbO_2 films as shown in Table 1. These films were obtained by depositing a [100] Tl_2O_3 prelayer followed by deposition of a 1 μm film in their respective solutions using the applied potentials shown. For $Pb_xTl_yO_z$ deposited at 70 mV vs SCE, the open circuit is similar to the measured open circuit for Tl_2O_3. As the lead content increases, the open circuit also increases, and films deposited at 260 mV vs SCE approach an open-circuit similar to a PbO_2 film. This indicates that each of the compositions of the Pb−Tl−O mixed oxides have a characteristic open-circuit potential which is different from the pure components, due to the varying Tl/Pb ratio within the films.

The linear sweep voltammetry and open circuit measurements for Pb−Tl−O films suggest that both kinetics and thermodynamics can affect the deposition from a single plating bath. Each composition should have a characteristic deposition potential. Consequently, it is difficult to calculate the film composition in advance using the current from the linear sweep scan

Table 2. Comparison of Bulk Film Compositions by Energy-Dispersive X-ray Spectroscopy (EDS) and Anodic Stripping Voltammetry (ASV)

deposition potential (mV vs SCE)	current density (mA/cm^2)	atomic percent Pb (ASV)	atomic percent Tl (ASV)	atomic percent Pb (EDS)	atomic percent Tl (EDS)
70	0.05	54	46	45	55
150	1.0	68	32	64	36
230	5.0	79	21	76	24

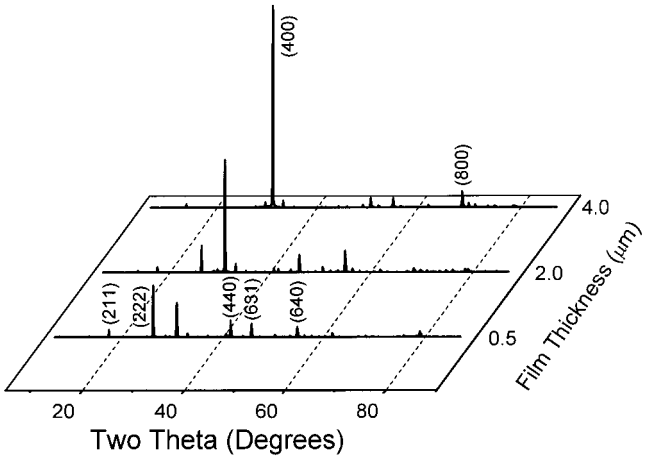

Figure 3. Dependence of the prelayer texture on the film thickness for a Tl_2O_3 prelayer. The texture increased with film thickness. A current density of 5 mA/cm^2, and a stirred solution of 0.1 M $TlNO_3$ in 5 M NaOH was used to deposit the prelayers.

in a multiple component solution such as 5 mM $TlNO_3$, 100 mM $Pb(NO_3)_2$ in 5 M NaOH. Instead, compositions for bulk films grown either galvanostatic or potentiostatic can be determined by X-ray spectroscopy or electrochemical analysis. The relative compositions of Pb−Tl−O films were first analyzed using energy-dispersive X-ray spectroscopy (EDS) in a scanning electron microscope (SEM). The EDS results were confirmed by anodic stripping voltammetry (ASV) for dissolved films using the method of standard additions. The Pb−Tl−O films were first dissolved in 50 mM ascorbic acid and the Pb(II) in solution was complexed with EDTA ($C_{10}H_{16}N_2O_2$) to shift the Pb(II) reduction peak to more cathodic potentials. The Tl(I) and Pb(II) were then preconcentrated from the solution into a mercury drop working electrode at −1.0 V versus Ag/AgCl. Following the preconcentration step, the ions were stripped electrochemically by anodically scanning the potential. The ASV results are compared to the EDS results in Table 2. These results confirm that the composition within these bulk films can be controlled with the applied potential or current during deposition.

Textured Prelayers. Prelayers of [210] oriented Pb−Tl−O and [100] oriented Tl_2O_3 were deposited onto stainless steel substrates at 5 mA/cm^2. The Pb−Tl−O prelayers had a fluorite crystal structure with space group $Fm3m$, and a lattice parameter of 0.5342 nm. The Tl_2O_3 prelayers had a bixbyite crystal structure with space group $Ia3$, and a lattice parameter of 1.0543 nm. The bixbyite structure is often described as a doubled fluorite structure with one-quarter of the oxygens missing. The mismatch between the doubled Pb−Tl−O and the Tl_2O_3 structure is 1.3%.

The evolution of texture for the prelayers is demonstrated in Figure 3 for a series of thallic oxide prelayers. By a thickness of 5 μm, Tl_2O_3 prelayers were mainly [100] oriented. For the Pb−Tl−O prelayer, the texture

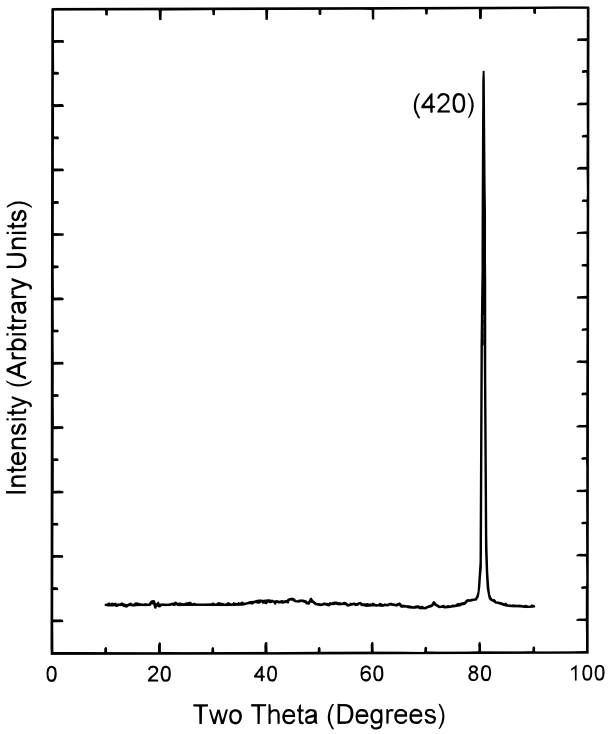

Figure 4. Highly oriented 20 μm Pb−Tl−O prelayer with a [210] texture. A current density of 5 mA/cm^2, and a stirred solution of 0.005 M $TlNO_3$, 0.1 M $Pb(NO_3)_2$ in 5 M NaOH was used to deposit the Pb−Tl−O film.

also increased as the film thickness increased. A Pb−Tl−O prelayer shown in Figure 4 has the (420) reflection as the main peak at a thickness of 20 μm. The high intensity of the (420) reflection relative to the other peaks in the X-ray spectrum is an indication of a strongly preferred orientation with the {210} planes parallel to the substrate surface. These textured prelayers were used as substrates for subsequent superlattice deposition.

The grain size for the textured prelayers was measured parallel to the stainless steel substrates on the surface of the films using the line-intercept method in scanning electron microscopy (SEM). Figure 5A shows the variation of grain size with film thickness for Tl_2O_3 prelayer films. The grain size increased from 0.25 μm at a film thickness of 0.5 μm to approximately 2 μm at a film thickness of 5 μm. The microstructure of the 5 μm thick Tl_2O_3 film shown in Figure 5B consists of faceted grains. The Tl_2O_3 films appear dense on the surface for a 5 μm thickness. The average grain size for the Pb−Tl−O prelayer also increases with the film thickness as shown in Figure 6A. Initially, the grain size was approximately 0.5 μm for a film thickness of 1 μm and increased to over 2 μm for a 20 μm thick film. As the film thickness increases to 20 μm, the grains appear rounded without obvious faceting as shown in Figure 6B.

We have characterized the oriented prelayers with X-ray diffraction using azimuthal rotation scans. These scans provide information on the texture parallel (i.e., in-plane) to the substrate.[20] Azimuthal scans are obtained by tilting the substrate to an appropriate angle such that another set of planes, which are an allowable

(20) Klug, H. P; Alexander, L. E. *X-ray Diffraction Procedures for Polycrystalline and Amorphous Materials,* 2nd ed.; John Wiley & Sons: New York, 1974.

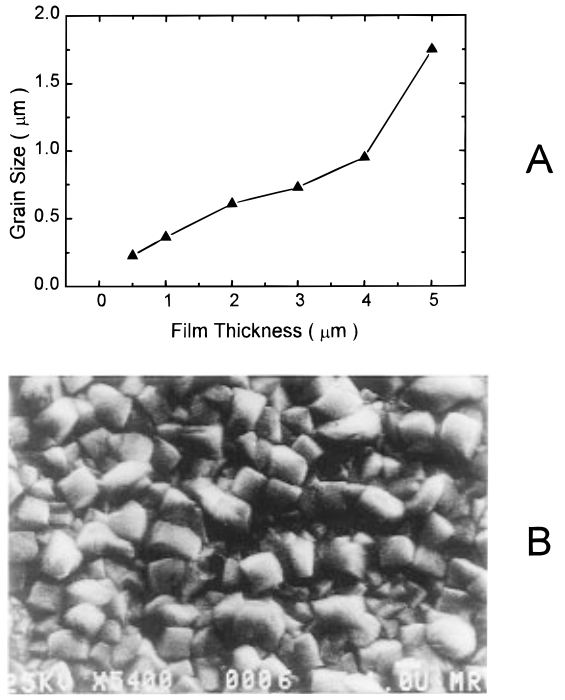

Figure 5. (A) Dependence of the average grain size with Tl_2O_3 film thickness. (B) Surface morphology of the [100] oriented oxide. The 5 μm thick film shows a faceted surface.

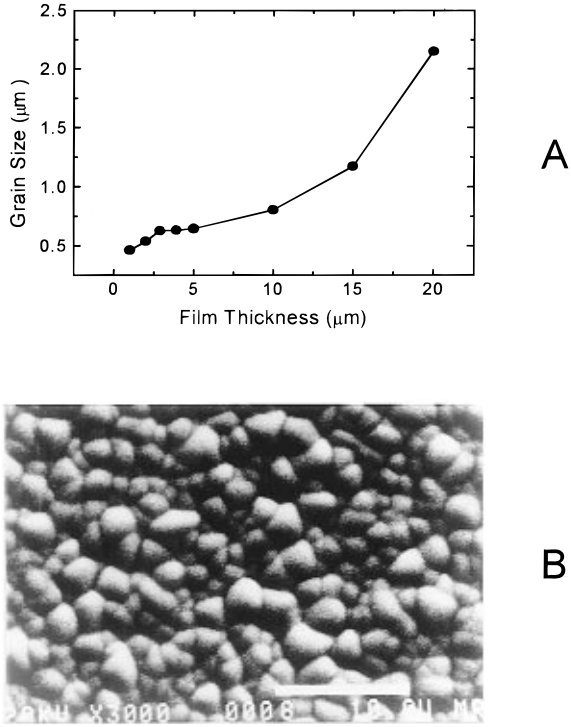

Figure 6. (A) Dependence of the average grain size with Pb−Tl−O film thickness. (B) Surface morphology of the [210] oriented oxide with a film thickness of 20 μm.

reflection for that structure, are positioned parallel to the substrate (in-plane position). The {111} planes satisfy this requirement for the electrodeposited prelayer films. The tilt angles were 39.2° for the [210] oriented mixed oxide and 54.7° for the [100] oriented thallic oxide. After tilting, the samples are rotated by a 360° azimuthal angle to determine if in-plane orientation exists. The tube and detector are positioned at the Bragg condition for the {111} planes. Figure 7 compares in-plane textures for (A) [100] silicon single

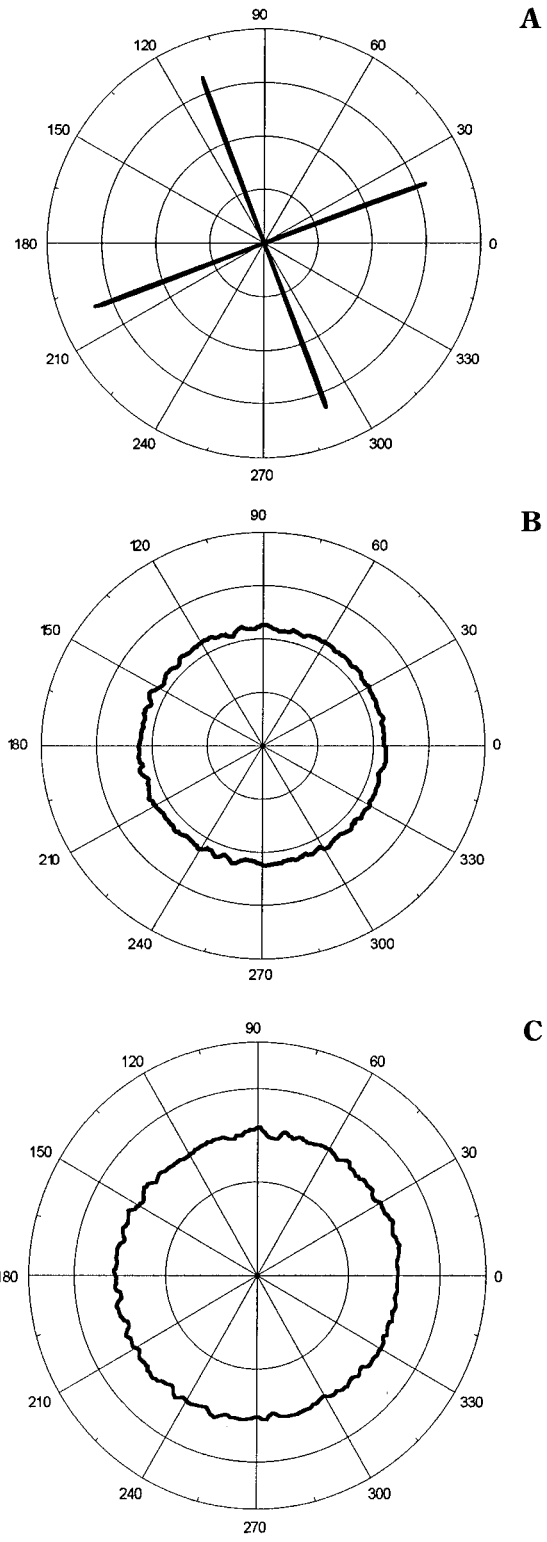

Figure 7. Rotational scans for (A) [100] silicon single crystal, (B) silicon powder, and (C) a 5 μm thick [100] Tl_2O_3 film. X-ray diffraction is from the {111} planes.

crystal, (B) silicon powder, and (C) a 5 μm thick Tl_2O_3 film. If in-plane texture exists, the symmetry for the {111} planes will be 4-fold, and the azimuthal scans will contain four maxima. This is demonstrated for single-crystal silicon by Figure 7A. A random sample, such as silicon powder, would not have distinct maxima as shown in Figure 7B. As seen in Figure 7C, the in-plane texture of the electrodeposited film was also random. Similar results are obtained for mixed oxide prelayers and the superlattices deposited onto these prelayers.

The microscopic or atomistic mechanisms which result in textured films are not universally understood. In general, the fastest growing direction approaches a perpendicular alignment with the original surface as the film growth proceeds. For electrodeposited films, the exchange current density, j_o, has been shown to vary for different crystal faces.[21] Deposition rates on different faces can be altered by adsorbed species such as hydrogen or organic additives. Also, a physically non-uniform surface can create a different current density at a specific point resulting in the alteration of the deposition rate. Electrodeposited films of Tl_2O_3 have a strong [100] texture, indicating the {100} planes have the fastest growth rate. In contrast, Wirtz and Siebert showed that the ⟨111⟩ directions were the fastest growing for bcc-Tl_2O_3 grown by vapor deposition.[22] There are other examples of electrodeposited films which also exhibit a [110] texture. Electrodeposited Cu/Ni superlattices have been fabricated primarily with a [110] texture.[23] These multilayers contain (110), (100), and (111) facets. The modulation wavelength was measured to be the largest on the (110) planes followed by the (100) and (111) planes. The texture of these electrodeposited films are in contrast to sputtered Fe/Pd superlattice films,[24] where the closest packed planes grow the fastest and are parallel to the substrate [i.e., (110) for bcc-Fe and (111) for fcc-Pd].

Superlattice Growth. Superlattices electrodeposited onto these prelayers in the Pb−Tl−O system consist of alternating layers, where one layer is stacked on top of another without a change in the crystallographic orientation normal to the substrate. The superlattice structures can be deposited by pulsing either the current or potential. Composition profiles have been calculated for potential pulsed superlattices.[1] Unless otherwise stated, the superlattices grown for this paper were made by pulsing the current density between 0.5 and 5.0 mA/cm^2. A schematic of a superlattice is shown in Figure 8. The individual layer thickness (λ_a or λ_b) in Figure 8 depend on the deposition times at the respective current densities for each layer. The thickness of layer a plus layer b equals the modulation wavelength, Λ, of the superlattice. For an electrochemically deposited film, the modulation wavelength, Λ, can be estimated from Faraday's law:

$$\text{moles} = \frac{Q}{nF} = \frac{1}{nF}\int_i^t i\,\mathrm{d}t = \frac{\rho A \lambda_F}{M} \qquad (1)$$

by rearranging eq 1 to

$$\lambda_F = MQ/nFA\rho \qquad (2)$$

and substituting from the following equations:

$$\Lambda_F = \lambda_{F,a} + \lambda_{F,b} \qquad (3)$$

$$n_a = n_b = n \qquad (4)$$

(21) Bockris, J. O'M.; Reddy, A. K. N. *Modern Electrochemistry*, 3rd ed.; Plenum Press: New York, 1977; Vol. 2.
(22) Wirtz, G. P.; Siebert, D. C. *J. Cryst. Growth* **1976**, *32*, 274.
(23) Haseeb, A. S. M. A.; Celis, J. P.; Roos, J. R. *J. Electrochem. Soc.* **1994**, *141*, 230.
(24) Boufelfel, A.; Emrick, R. M. *Phys. Rev. B* **1991**, *43*, 13, 152.

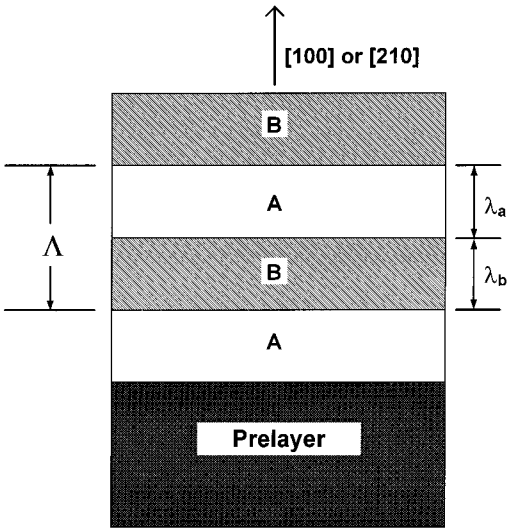

Figure 8. Idealized superlattice grown on an oriented prelayer. The orientation of the prelayer is maintained through the superlattice. The thickness of layer a is λ_a, and the thickness of layer b is λ_b.

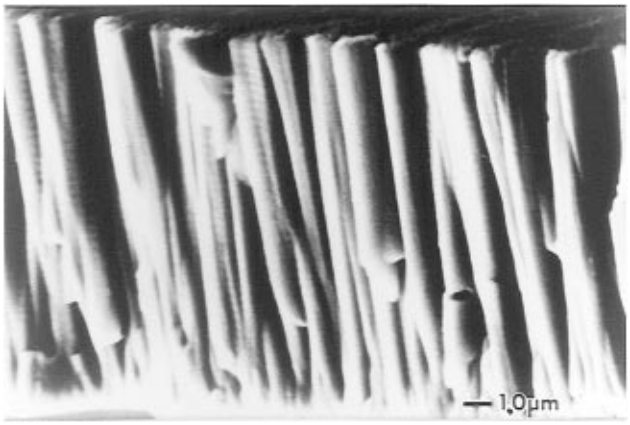

Figure 9. Scanning electron micrograph of an electrodeposited columnar superlattice structure. The individual layer thicknesses are approximately 0.5 μm. The bar marker is 1.0 μm.

then the equation for the modulation wavelength is

$$\Lambda_F = \frac{1}{nFA}\left(\frac{Q_a M_a}{\rho_a} + \frac{Q_b M_b}{\rho_b}\right) \quad (5)$$

For galvanostatically deposited superlattices, the charge for the individual layer Q_i, is replaced by the product (it) which results in:

$$\Lambda_F = \frac{1}{nFA}\left(\frac{i_a t_a M_a}{\rho_a} + \frac{i_b t_b M_b}{\rho_b}\right) \quad (6)$$

where n is the number of electrons transferred, F is Faraday's number, A is the electrode area, i is the applied current, t is the dwell time, M is the formula weight, and ρ is the density.

A cleaved cross section of a Pb−Tl−O modulated film was grown with layer thicknesses on the order of 0.5 μm for imaging with the SEM. Deposition was accomplished by growing an oriented prelayer followed by pulsing the potential between 70 and 230 mV vs SCE for superlattice growth. The SEM image of this modulated film is shown in Figure 9. The Pb−Tl−O film grows as a columnar structure. The superlattices deposited by either potential or current control all have columnar grains that grow perpendicular to the substrate.

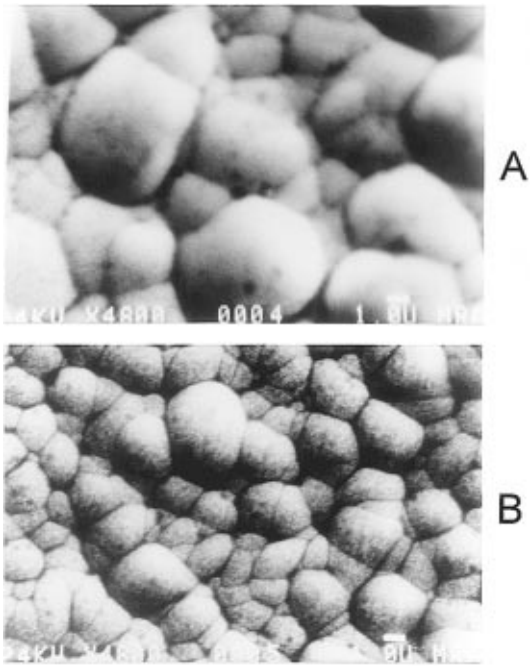

Figure 10. (A) Surface morphology of a [100] textured superlattice grown on [100] Tl_2O_3. The faceting from the prelayer was not observed on the surface of the superlattice. (B) Surface morphology of a [210] textured superlattice without the presence of facets. Both superlattices were grown by current pulsing. The thicknesses of the superlattices were 6 and 4.5 μm for the [100] and [210] textures, respectively.

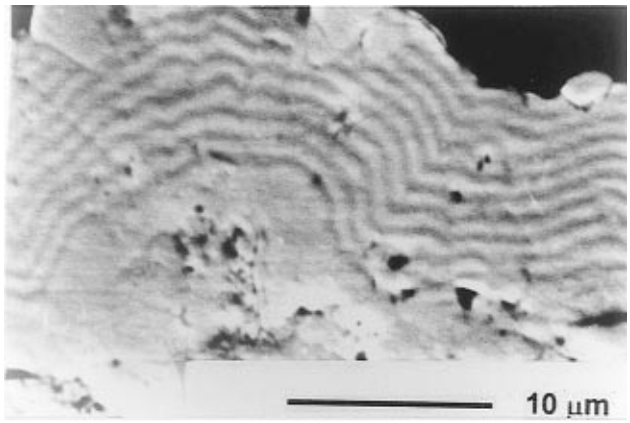

Figure 11. Polished cross section of a scanning electron micrograph of a superlattice. The superlattice maintains the two-dimensional growth around the three-dimensional defect in the sublayer. The bar marker is 10 μm.

It is interesting to compare the surface morphologies of the textured prelayers to that of the superlattices. The surfaces of a [100] textured superlattice and a [210] textured superlattice are shown in Figure 10A,B, respectively. In both cases, the grains appear rounded and facets are not observed. However, the surface morphology of the [100] oriented Tl_2O_3 prelayer was faceted while the [210] oriented Pb−Tl−O prelayer had rounded grains (Figures 5 and 6). Figure 11 shows a polished cross section of an electrodeposited Pb−Tl−O superlattice with an individual layer thickness of 0.65 μm imaged in the SEM. A three-dimensional defect is shown in the sublayer. The alternating layer sequence is preserved around the sublayer defect.

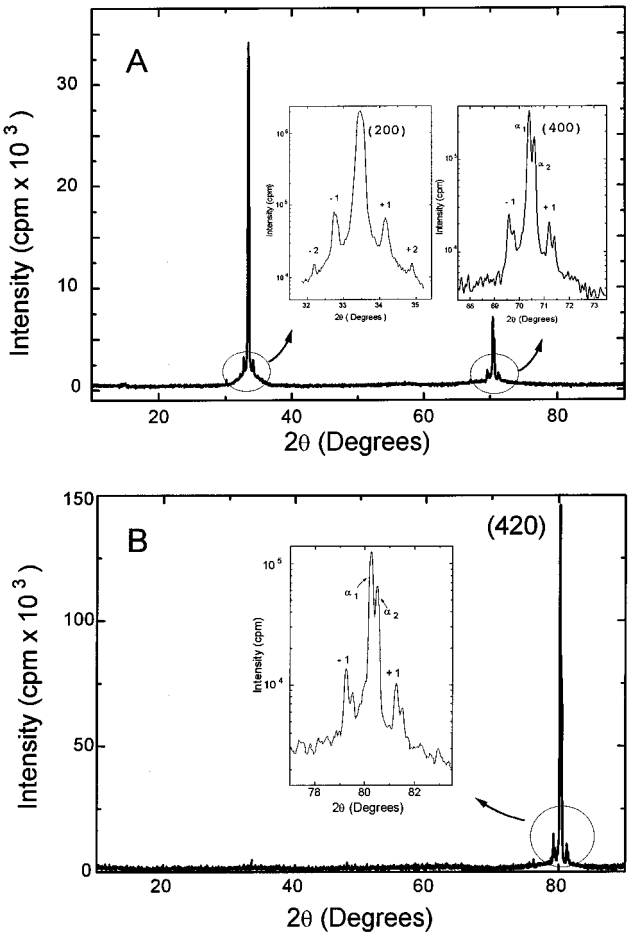

Figure 12. (A) [100]-textured superlattice in the Pb−Tl−O system. The modulation wavelength was calculated as Λ_F = 13.2 nm by Faraday's law and measured by X-ray diffraction as Λ_x = 13.3 nm. (B) [210]-textured superlattice with Λ_F = 12 nm and Λ_x = 11.8 nm. Both superlattices were deposited by pulsing the current between 0.05 mA/cm^2 (82 s) and 5 mA/cm^2 (1.2 s).

Structural evidence of a superlattice is shown by satellites which are symmetric around a Bragg reflection. Satellites result from a periodic variation in lattice spacing or composition.[25] The periodic variation can be represented as a waveform. For waveforms that vary sinusoidally, first-order satellites are expected. As the waveform becomes more square, higher orders of satellites are possible. For a perfect square wave (rarely observed), only odd orders of satellites are expected. When the lattice spacing and composition both vary periodically, the intensities of like orders of satellites are not equal. The scattering factor is said to be convoluted with lattice spacing variation. An example of [210] and [100] textured superlattices grown by current pulsing are shown in Figure 12. Notice that there are first-order satellites present around each main Bragg reflection (shown in the insert boxes of Figure 12). These satellites give structural evidence that the electrodeposited films are indeed superlattices. Also, from Figure 12, unequal satellite intensities are observed in the first-order satellites for both the [100] and [210] textured superlattices.

For a superlattice, the repeat distance or modulation wavelength creates an artificial interplanar spacing that

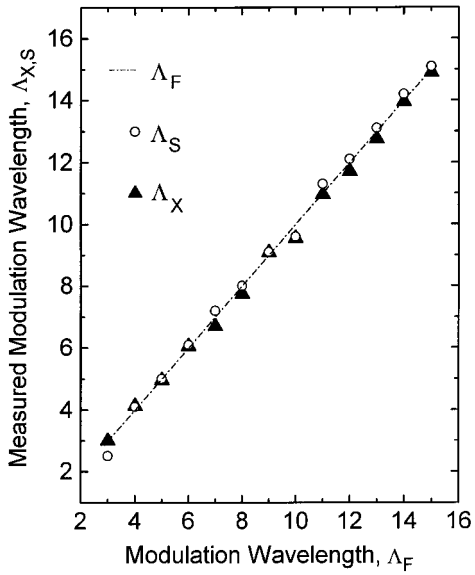

Figure 13. Comparison of the Pb−Tl−O superlattice modulation wavelength in nanometers calculated by Faraday's law (Λ_F) with those measured by scanning tunneling microscopy (Λ_S) and X-ray diffraction (Λ_X).

is not present in the bulk materials. These planes scatter X-rays similar to a bulk crystal, where the scattering from the *i*th plane can be represented by

$$L_i\lambda = 2\Lambda \sin \theta_i \tag{7}$$

For two planes i and j separated by a distance Λ, the path difference is:[26]

$$(L_i - L_j)\lambda = 2\Lambda(\sin \theta_i - \sin \theta_j) \tag{8}$$

Or in terms of the modulation wavelength for X-ray diffraction, $\Lambda = \Lambda_x$:

$$\Lambda_x = \frac{(L_i - L_i)\lambda}{2(\sin \theta_i - \sin \theta_j)} \tag{9}$$

where L_i and L_j are the satellite orders, θ_i and θ_j are the satellite positions, and λ is the wavelength of the X-ray radiation.

The scanning tunneling microscope (STM) has also been used to directly measure the periodicity and modulation wavelengths of cleaved cross sections of Pb−Tl−O superlattices.[27] A comparison of modulation wavelengths measured by XRD (Λ_x) and STM (Λ_S) to those calculated from the integrated charge (Λ_F) is shown in Figure 13. The modulation wavelengths determined from the integrated charge were calculated assuming theoretical density and 100% current efficiency. The modulation wavelengths measured by XRD and STM agree for superlattice layers grown as small as 3 nm to that calculated from the integrated charge. Since the Faradaic calculations assume theoretical density, it is unlikely that the agreement would be as good if the films grew three-dimensionally instead of two-dimensionally.

As the individual layer thickness increased beyond 10 nm (Λ = 20 nm), the X-ray diffraction pattern became more complicated. Figure 14A shows the X-ray

(25) Guiner, A. *X-ray Diffraction in Crystals, Imperfect Crystals and Amorphous Bodies*, 1st ed.; W. H. Freeman & Co.: San Francisco, 1963.

(26) Schuller, I. K. *Phys. Rev. Lett.* **1980**, *44*, 1597.

(27) Golden, T. D.; Raffaelle, R. P.; Switzer, J. A. *Appl. Phys. Lett.* **1993**, *63*, 1501.

Table 3. X-ray Powder Diffraction Results for Bulk Films Grown under Galvanostatic Control

applied current density (mA/cm^2)	measured potential (mV vs SCE)	lattice parameter[a] (nm)	d spacing (hkl = 420) (Å)	I/I_0 (%) (hkl = 420)	theor density[b] (g/cm^2)
0.05	70	0.5328	1.191	6	10.45
1.0	150	0.5338	1.193	12	10.39
5.0	230	0.5342	1.195	21	10.39

[a] Determined from the (531) reflection. [b] Based on the measured atomic percents from EDS and assuming all lead and thallium ions are +4 and +3, respectively.

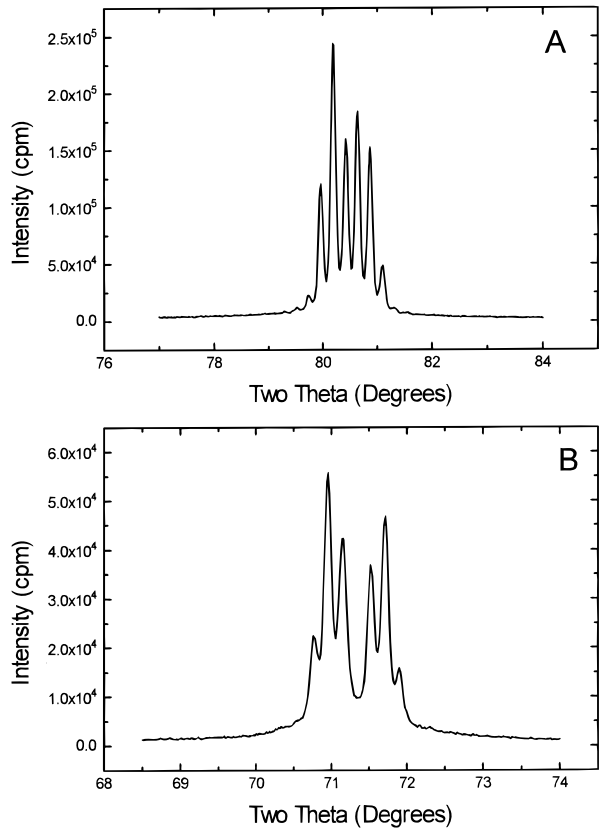

Figure 14. (A) X-ray diffraction pattern of a [210]-textured superlattice in the Pb−Tl−O system using Cu Kα radiation as the X-ray source. The modulation wavelength was calculated as $\Lambda_F = 50$ nm by Faraday's law. (B) Same as (A), except using Cu Kβ radiation for the X-ray source.

diffraction pattern for a Pb−Tl−O superlattice with a modulation wavelength of 50 nm. The diffraction pattern for this superlattice was obtained using the same energy wavelength (Cu Kα_1/Cu Kα_2) as in Figure 12. Notice for the superlattices in Figure 12 that Kα_1 and Kα_2 appear for each peak in the X-ray diffraction patterns. Since the energy resolution of the Si−Li solid-state detector is 150 eV and the Kα_1/Kα_2 doublet is separated by only 20 eV, the detector cannot discriminate between the Kα_1 and Kα_2 peaks. Due to the presence of this doublet in Figure 14A, it is difficult to interpret the X-ray pattern. To obtain a simpler pattern, Cu K$_\beta$ radiation was used instead to obtain the X-ray pattern for the sample in Figure 14A. Figure 14B shows the X-ray pattern for the same superlattice as in Figure 14A using Cu Kβ radiation as the X-ray source. In the X-ray pattern a splitting of the main Bragg peak occurs into two Bragg peaks with individual satellites on each side of the Bragg peak. The two Bragg peaks represent layers A and B of the superlattice grown by alternating the applied current density between 0.05 and 5.0 mA/cm^2. The Bragg peak at lower 2θ in Figure 14B has a calculated d spacing of 1.195 Å while the higher 2θ peak d spacing peak is 1.191 Å. The d spacings for the two Bragg peaks can be compared to the d spacings for individual bulk films in Table 3. The lower 2θ Bragg peak in Figure 14B corresponds to the 5.0 mA/cm^2 layer, and the higher 2θ Bragg peak corresponds to the 0.05 mA/cm^2 layer. This splitting of the Bragg peak may be due to a relaxation in the individual layers of the superlattice. Relaxation is expected in a strained-layer superlattice when the modulation wavelength exceeds a critical value. The lattice mismatch in this system is approximately 0.3%. The critical modulation wavelength would be expected to be smaller for superlattices with a larger mismatch. Also as the modulation wavelength increases beyond 50 nm, the peak for the 5.0 mA/cm^2 layer increases in intensity compared to the peak for the 0.05 mA/cm^2 layer. The higher intensity for the 5.0 mA/cm^2 layer of the (420) reflection is also seen for the powder patterns of bulk films in Table 3. Our results suggest that partial relaxation of coherency occurs when the modulation wavelength exceeds 20 nm. At modulation wavelengths greater than 50 nm, the lattice parameters for the individual layers have relaxed to the values observed in bulk films grown at the respective current densities.

Conclusions

Electrodeposition was used to deposit superlattices in the Pb−Tl−O system using either current or potential pulsing. The modulation wavelengths calculated from Faraday's law agreed well with the values determined by X-ray diffraction and scanning tunneling microscopy. The superlattices grew epitaxially and were textured perpendicular to the substrate by deposition onto either [100] oriented Tl_2O_3 or [210] oriented Pb−Tl−O. The prelayers and superlattices did not possess in-plane texture. Increasing texture and grain growth was observed in the prelayers perpendicular to the substrate as the films became thicker. The [100] oriented Tl_2O_3 prelayer films were faceted while the [210] oriented Pb−Tl−O prelayers contained rounded grain shapes. Deposition of superlattices onto either of these prelayers resulted in grains which appear to be nonfaceted by SEM. Partial relaxation of coherency in the superlattice was observed for modulation wavelengths exceeding about 20 nm.

Acknowledgment. This work was supported in part by the National Science Foundation Grant No. DMR-9202872, the Office of Naval Research Grant No. N00014-96-1-0984 and N00014-94-1-0917, and the University of Missouri Research Board.
CM970074I